

# Numerical Method for Eulerian Vlasov Simulation Based on Multi-Moment Scheme<sup>\*)</sup>

Takafumi KAWANO, Kenji IMADERA, Jiquan LI and Yasuaki KISHIMOTO

*Department of Fundamental Energy Science, Graduate School of Energy Science,  
Kyoto University, Gokasho, Uji, Kyoto 611-0011, Japan*

(Received 10 December 2010 / Accepted 7 March 2011)

A new scheme referred to as the multi-moment (MM) scheme is explored to develop a more reliable Vlasov code from the viewpoint of numerical properties. The MM scheme is based on the Eulerian approach, where spatial derivatives are evaluated by interpolation functions locally constructed by not only grid values but also 0th-, 1st-, and 2nd-order moment values between grids, which largely increases numerical accuracy and resolution. Through the Fourier analyses and benchmark tests of one-dimensional (1D) and 2D transport simulations, it is found that the MM scheme exhibits significantly smaller numerical dissipation and dispersion even near the Nyquist wave-number, and as a result, the MM scheme decreases the numerical cost. The MM scheme is also applied to a 1D Vlasov-Poisson simulation and we find that the scheme captures finer scale structure in velocity space compared to the conservative form of interpolated differential operator (IDO-CF) scheme, while also maintaining good energy conservation.

© 2011 The Japan Society of Plasma Science and Nuclear Fusion Research

Keywords: Vlasov-Poisson simulation, conservative numerical scheme, multi-moment scheme

DOI: 10.1585/pfr.6.2401097

## 1. Introduction

Nonlinear gyrokinetic and driftkinetic Vlasov simulations [1], which avoid directly solving the fast motion processes of particles with cyclotron frequencies while maintaining important kinetic effects, are considered to be an essential tool for the study of turbulent transport driven by micro-scale instabilities. Although several gyrokinetic simulations have adopted a Lagrangian (particle) approach because of limited computational resources, the Eulerian (mesh) approach is superior in reducing numerical noise and extending to an open system. Recently, with the aid of rapid progress in high-performance computing and advanced numerical schemes in CFD field, the Eulerian approach has become more popular in gyrokinetic simulations.

Several numerical schemes have been developed for solving the Vlasov equation. A splitting scheme [2] is one candidate; however, the scheme can induce a phase error associated with convection in the gyrokinetic simulation because of the nature of the semi-Lagrangian approach.

Recently, an alternative approach referred to as the conservative form of interpolated differential operator (IDO-CF) scheme [3] has been applied [4]. This scheme is based on the Eulerian approach and ensures rigorous conservation of the integrated value over the whole system, so that the scheme can be applied to problems that require simulations over a long time scale.

In this paper, we explored the multi-moment (MM) scheme based on the IDO-CF one. In this scheme, spatial derivatives are evaluated by interpolation functions, which is similar in concept to the IDO-CF scheme. However, in the MM scheme, not only grid and cell-integrated (0th-order moment) values, but also 1st- and 2nd-order moment values between the grids are used and time-integrated as independent variables. This feature largely improves numerical accuracy and resolution. Through the Fourier analyses [5,6] and benchmark tests of the one-dimensional (1D) and 2D transport simulations, it is found that the MM scheme exhibits significantly reduced numerical dissipation and dispersion even near the Nyquist wave-number. We also applied the MM scheme to a 1D Vlasov-Poisson simulation and found that it captures finer scale structure in velocity space compared to the IDO-CF scheme.

This paper has the following outline. In Sec. 2, the numerical procedure of the MM scheme is briefly described. Then, we perform the Fourier analyses (in Sec. 3) and 1D (in Sec. 4) and 2D (in Sec. 5) benchmark tests to investigate the numerical properties of the MM scheme. The application of the MM scheme to the 1D Vlasov simulation is discussed in Sec. 6. Finally, the results are summarized with short remarks in Sec. 7.

author's e-mail: kawano@center.iae.kyoto-u.ac.jp

<sup>\*)</sup> This article is based on the presentation at the 20th International Toki Conference (ITC20).

## 2. Numerical Method of the MM Scheme

In this section, we describe the principal concept of the MM scheme based on a numerical procedure to solve the 1D transport equation, given as

$$\frac{\partial f(t, x)}{\partial t} + \frac{\partial}{\partial x} [uf(t, x)] = 0, \quad (1)$$

where  $t$  denotes the time,  $x$  the spatial coordinate,  $u$  the velocity and  $f$  the transported quantity. Here,  $u$  is assumed to be constant. A simulation box is partitioned into cells  $x_j = j\Delta x = jL_x/N_x (j = 1, 2, \dots, N_x)$ , where  $L_x$  and  $N_x$  are the spatial periodic length and the number of mesh points, respectively. Let  ${}^m M_{j+1/2}$  ( $m = 0, 1, 2$ ) be the value of each moment between  $x_j$  and  $x_{j+1}$  defined as

$${}^0 M_{j+1/2} = \int_{x_j}^{x_{j+1}} f dx / \Delta x, \quad (2)$$

$${}^1 M_{j+1/2} = \int_{x_j}^{x_{j+1}} (x - x_j) f dx / \Delta x^2, \quad (3)$$

$${}^2 M_{j+1/2} = \int_{x_j}^{x_{j+1}} (x - x_j)^2 f dx / \Delta x^3, \quad (4)$$

where  $m$  corresponds to the order of the moment. The  $i$ -th piece of the interpolation function  $F_j(x)$  is constructed over upwind stencils. By considering  $u < 0$ , a left-bias interpolation can be written as

$$F_j(x) = a(x - x_j)^4 + b(x - x_j)^3 + c(x - x_j)^2 + d(x - x_j) + e. \quad (5)$$

By using the five constraints for the interpolation given as

$$\begin{aligned} F_j(x_j) &= f_j, \\ F_j(x_{j+1}) &= f_{j+1}, \\ \int_{x_j}^{x_{j+1}} F_j(x) dx / \Delta x &= {}^0 M_{j+1/2}, \\ \int_{x_j}^{x_{j+1}} (x - x_j) F_j(x) dx / \Delta x^2 &= {}^1 M_{j+1/2}, \\ \int_{x_j}^{x_{j+1}} (x - x_j)^2 F_j(x) dx / \Delta x^3 &= {}^2 M_{j+1/2}, \end{aligned} \quad (6)$$

the polynomial (5) is completely determined and the coefficients are obtained as

$$\begin{aligned} a &= 35(f_j + f_{j+1} - 12{}^0 M_{j+1/2} + 60{}^1 M_{j+1/2} \\ &\quad - 60{}^2 M_{j+1/2}) / \Delta x^4, \\ b &= -20(4f_j + 3f_{j+1} - 45{}^0 M_{j+1/2} + 216{}^1 M_{j+1/2} \\ &\quad - 210{}^2 M_{j+1/2}) / \Delta x^3, \\ c &= 30(2f_j + f_{j+1} - 20{}^0 M_{j+1/2} + 90{}^1 M_{j+1/2} \\ &\quad - 84{}^2 M_{j+1/2}) / \Delta x^2, \\ d &= -4(4f_j + f_{j+1} - 30{}^0 M_{j+1/2} + 120{}^1 M_{j+1/2} \\ &\quad - 105{}^2 M_{j+1/2}) / \Delta x, \\ e &= f_j. \end{aligned} \quad (7)$$

The time derivatives of the independent values are computed as

$$\left( \frac{\partial f}{\partial t} \right)_j = -u \frac{\partial f}{\partial x} \Big|_{x=x_j} = -u \frac{\partial F_j(x)}{\partial x} \Big|_{x=x_j}, \quad (8)$$

$$\left( \frac{\partial {}^0 M}{\partial t} \right)_{j+1/2} = -u \int_{x_j}^{x_{j+1}} \frac{\partial f}{\partial x} dx / \Delta x = -u \frac{f_{j+1} - f_j}{\Delta x}, \quad (9)$$

$$\left( \frac{\partial {}^1 M}{\partial t} \right)_{j+1/2} = -u \frac{f_{j+1} - {}^0 M_{j+1/2}}{\Delta x}, \quad (10)$$

$$\left( \frac{\partial {}^2 M}{\partial t} \right)_{j+1/2} = -u \frac{f_{j+1} - {}^2 M_{j+1/2}}{\Delta x}. \quad (11)$$

According to Eqs.(8-11), we can advance each value in time by using typical numerical methods such as the Runge-Kutta scheme. Note that Eq.(9) is expressed in flux form, so that  $\sum_j {}^0 M_{j+1/2}$  becomes constant for all time-steps. As a result, the present scheme is superior in investigating the problems that require simulations over a long time scale.

## 3. Fourier Analysis of the MM Scheme

In this section, we present the Fourier analysis [5,6] of the MM scheme to evaluate stability and accuracy in solving the 1D transport equation given by Eq.(1). When the spatial profile of a transported quantity is periodic over a domain with a uniform grid width, its grid value is decomposed into a Fourier series

$$f_j^n = \sum_k \hat{f}^n(k) \exp(ikx_j), \quad (12)$$

where  $i = \sqrt{-1}$  and  $k$  is the wave-number. In the MM scheme, each moment value is also decomposed as

$${}^0 M_{j+1/2}^n = \sum_k {}^0 \hat{M}^n(k) \exp(ikx_j) [\exp(ik\Delta x) - 1], \quad (13)$$

$${}^1 M_{j+1/2}^n = \sum_k {}^1 \hat{M}^n(k) \exp(ikx_j) [\exp(ik\Delta x) - 1], \quad (14)$$

$${}^2 M_{j+1/2}^n = \sum_k {}^2 \hat{M}^n(k) \exp(ikx_j) [\exp(ik\Delta x) - 1]. \quad (15)$$

In terms of Eqs.(8-11) and Eqs.(12-15), the discretized form of the time marching by the 4th-order Runge-Kutta method is written as

$$\mathbf{F}^{n+1} = \mathbf{F}^n + \sum_p^4 \beta_p \mathbf{A} \mathbf{F}_p^n \Delta t \equiv \mathbf{S} \mathbf{F}^n, \quad (16)$$

$$\mathbf{F}_p^n = \mathbf{F}^n + \sum_q^4 \alpha_{pq} \mathbf{A} \mathbf{F}_q^n \Delta t, \quad (17)$$

where  $n$  and  $p$  denote the time-step index and the stage number of the Runge-Kutta scheme, respectively.  $\alpha_{pq}$  and  $\beta_p$  are weighted coefficients given as  $\alpha_{21} = \alpha_{32} = 1/2$ ,  $\alpha_{43} = 1$ ,  $\beta_1 = \beta_4 = 1/6$ ,  $\beta_2 = \beta_3 = 1/3$  and  $\alpha_{pq} = 0$  for other components. The matrix  $\mathbf{F}^n$  and  $\mathbf{A}$  are given by

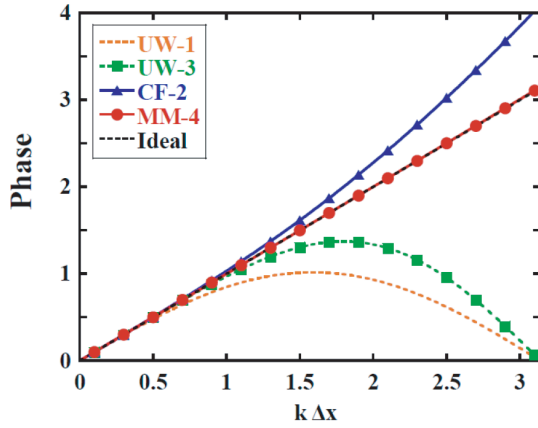


Fig. 1 Phase error of different schemes for the 1D linear transport equation. The red curve corresponds to the MM scheme, other curves correspond to the 1st-order upwind (orange), 3rd-order upwind (green), IDO-CF (blue) schemes, and ideal phase (black).

$$\mathbf{F}^n = \begin{pmatrix} \hat{f}^n(k) \\ {}^0\hat{M}^n(k) \\ {}^1\hat{M}^n(k) \\ {}^2\hat{M}^n(k) \end{pmatrix}, \quad (18)$$

$$\mathbf{A} = \begin{pmatrix} 1 + 4C[\exp(ik\Delta x) + 4] & -120C & 480C & -420C \\ -C[\exp(ik\Delta x) - 1] & 1 & 0 & 0 \\ -C \exp(ik\Delta x) & C & 1 & 0 \\ -C \exp(ik\Delta x) & 0 & 2C & 1 \end{pmatrix}, \quad (19)$$

where  $C = |u|\Delta t/\Delta x$  denotes the Courant number. Then, we obtain the matrix after  $n$  time-steps as

$$\mathbf{F}^n = \mathbf{S}\mathbf{F}^{n-1} = \mathbf{S}^2\mathbf{F}^{n-2} = \dots = \mathbf{S}^n\mathbf{F}^0. \quad (20)$$

To estimate the numerical dissipation and dispersion of each scheme, we define an amplification factor after  $n$  timesteps as

$$g(k) = |g_n(k)| \exp(i\theta_n) = \frac{\hat{f}^n(k)}{\hat{f}^0(k)}, \quad (21)$$

where  $|g_n|$  and  $\theta_n$  represent the gain and phase, respectively. The exact solution of the gain is unity, and the exact phase is  $\theta_n = Ckn\Delta x$ .

We examine the phase for various upwind schemes using the 4th-order Runge–Kutta time integration. Figure 1 shows the phase for the 1st- and 3rd-order upwind, IDO-CF, and MM schemes. The phase is normalized as  $\bar{\theta}_n = \theta_n/Cn$ , where the Courant number and the iteration number are set by  $C = 0.1$  and  $n = 1000$ , respectively. It is found that the MM scheme provides an accurate phase for a wide range of wave numbers in comparison with the conventional upwind schemes. Even at the Nyquist wave-number, the numerical phase error is found to be 3.1405. The normalized gain, defined as  $|\bar{g}_n| = |g_n|^{1/Cn}$ , is also shown in Fig. 2. The gains of all schemes are less than unity for the entire region of the wave number, which ensures numerical stability. At the Nyquist wave-number, the

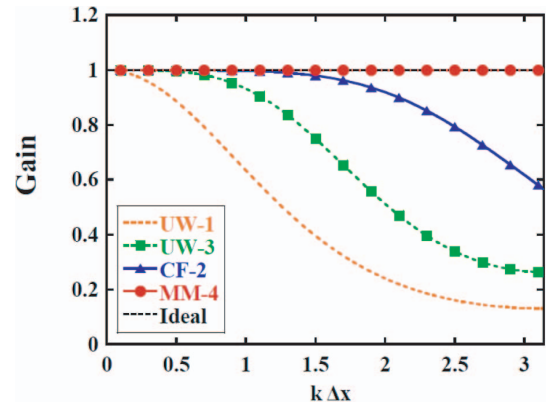


Fig. 2 Gain errors of different schemes for the 1D linear transport equation. The correspondence of each curve is the same as in Fig. 1.

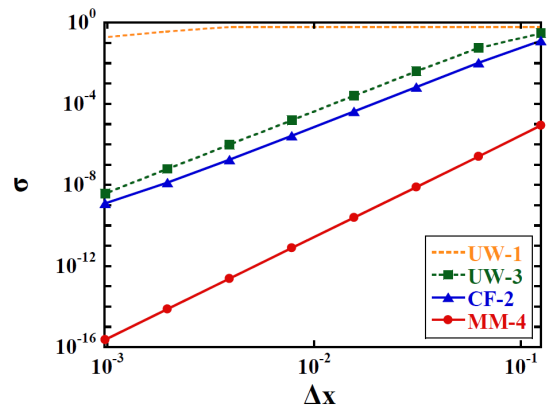


Fig. 3 Spatial accuracy of the numerical solution for the 1D transport equation by using the 1st-order upwind (orange), 3rd-order upwind (green), IDO-CF (blue), and MM schemes (red).

numerical gain error is found to be 0.99537. Thus, the MM scheme can achieve almost the same gain and phase as the ideal solutions, exhibiting much less dissipation and dispersion than the other schemes.

## 4. Application to the 1D Transport Simulation

To check the accuracy of the numerical solution, we applied the MM scheme incorporated with the 4th-order Runge–Kutta scheme to the 1D transport simulation, in which the governing equation is given by Eq. (1). We set the initial condition as  $f(t = 0, x) = 2 + \sin(2\pi x)$  for  $0 \leq x \leq 1$  and the CFL number as  $C = 0.1$ . Figure 3 shows the relative numerical error  $\sigma$  of each upwind scheme, i.e., 1st-order upwind, 3rd-order upwind, IDO-CF, and MM scheme, where  $\sigma$  is defined as

$$\sigma = \sum_{j=1}^{N_x} \frac{|f_j^{Num} - f_j^{True}|}{|f_j^{True}|}. \quad (22)$$

It is found that the error of the MM scheme has a convergence of  $\Delta x^5$ , whereas that of the IDO-CF scheme is  $\Delta x^3$ .

This accuracy corresponds to the order of the integral for each interpolation function. We also found that the MM scheme can achieve the same accuracy at approximately one-order smaller numerical cost.

### 5. Application to the 2D Transport Simulation

We also applied the MM scheme to the 2D linear transport simulation, in which the governing equation is given by

$$\frac{\partial f(t, x, y)}{\partial t} + \frac{\partial}{\partial x}[u(x, y)f(t, x, y)] + \frac{\partial}{\partial y}[v(x, y)f(t, x, y)] = 0. \tag{23}$$

First, we test the case with uniform velocity  $u(x, y) = v(x, y) = 1$ . The initial condition is set as

$$f(t = 0, x, y) = 2 + \sin(2\pi x) \sin(2\pi y). \tag{24}$$

Figure 4 shows the relative numerical error  $\sigma$  of each upwind scheme, i.e, 3rd-order upwind, IDO-CF and MM scheme. It can be seen that the MM scheme has a convergence of  $\Delta x^4$ .

We also test the 2D solid-body rotation problem called the Zalesak problem [7]. The solid body, whose initial profile is shown in Fig. 5 (a), rotates with the velocity field

given by  $u(x, y) = -2\pi y, v(x, y) = 2\pi x$ . All the computational conditions are assumed to be the same as those in Ref. [7]. Figure 5 (d) shows the profile after 10 complete revolutions with the MM scheme. For comparison, the numerical results with the 3rd-order upwind and IDO-CF schemes are also shown in Fig. 5 (b) and (c), respectively. We can see that the MM scheme gives a less diffusive result for the Zalesak problem.

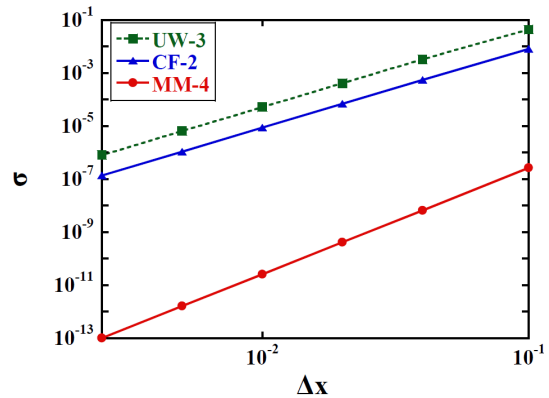


Fig. 4 Spatial accuracy of the numerical solution for the 2D transport equation by using the 3rd-order upwind (green), IDO-CF (blue), and MM schemes (red).

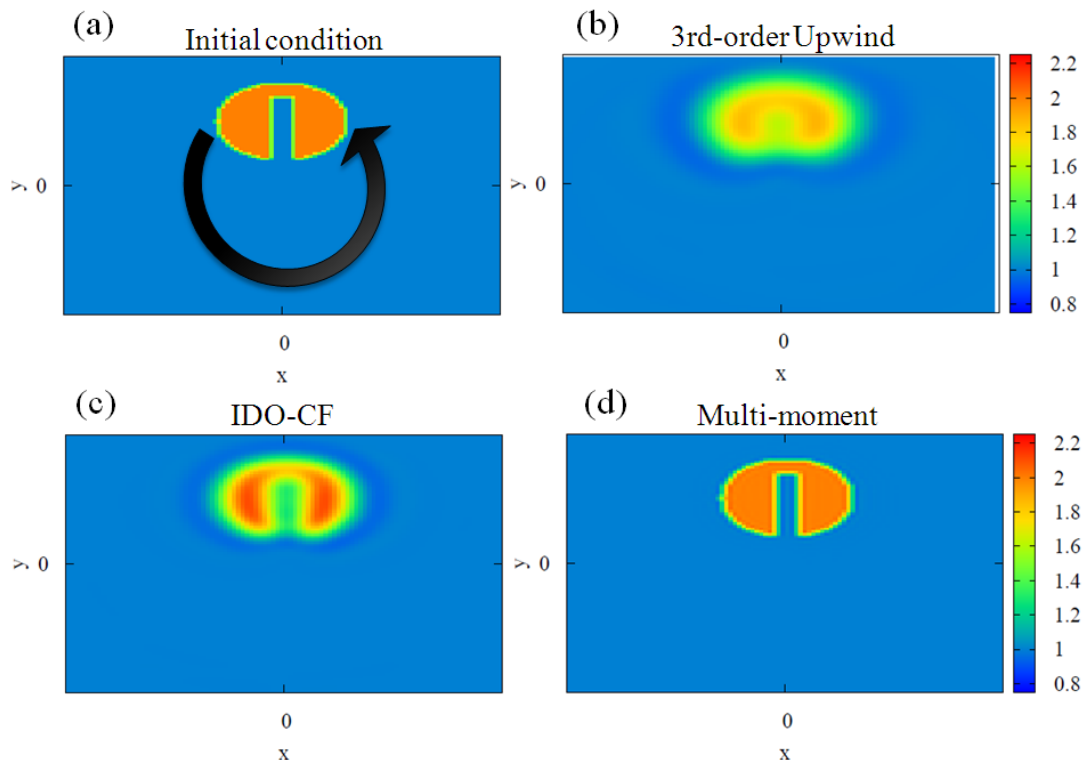


Fig. 5 Contour view of (a) the solid-body in the Zalesak problem after 10 anticlockwise rotations simulated by using the (b) 3rd-order upwind, (c) IDO-CF and (d) MM schemes. Here,  $100 \times 100$  mesh number and velocity field  $u(y) = -2\pi x, v(x) = 2\pi y$  are assumed. Grid points inside the cylinder have  $f = 2.0$ . All others have  $f = 1.0$ .

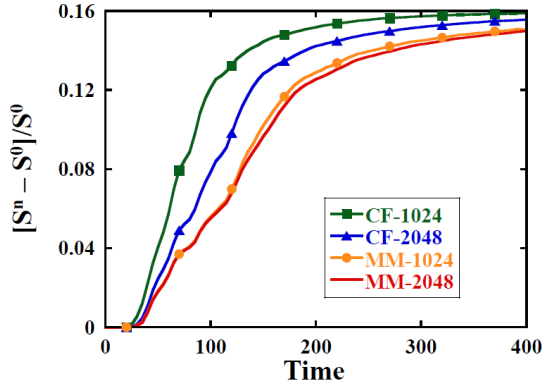


Fig. 6 Deviation from the initial values of the entropy defined as  $S^n = -\sum_{i,j} f_{i,j}^n \ln f_{i,j}^n \Delta x \Delta v$  by the IDO-CF and MM schemes with  $N_v = \{1024, 2048\}$ .

## 6. Application to the 1D Vlasov-Poisson Simulation

Finally, we applied the MM scheme to the 1D Vlasov-Poisson simulation, which has 1D in real space and 1D in velocity space. Let us consider the normalized 1D Vlasov-Poisson equations as

$$\frac{\partial f}{\partial t} + v \frac{\partial f}{\partial x} + \frac{\partial \phi}{\partial x} \frac{\partial f}{\partial v} = 0, \quad (25)$$

$$\frac{\partial^2 \phi}{\partial x^2} = \int_{-\infty}^{+\infty} f dv - 1, \quad (26)$$

where  $f$  and  $\phi$  denote the distribution function for electrons and the electrostatic potential, respectively; stationary background ions are assumed. The computational domain is defined in  $0 \leq x \leq L_x$  and  $-v_{\max} \leq v \leq v_{\max}$  with a periodic boundary condition in the  $x$ -direction and is discretized by numerical grid points of  $(N_x, N_v - 1)$ .

Here, we investigate a benchmark test for nonlinear Landau damping with the initial condition

$$f(t=0, x, v) = \frac{1}{2\pi} \exp\left(-\frac{v^2}{2}\right) \left(1 + A \cos \frac{2\pi}{L_x} x\right), \quad (27)$$

where  $L_x = 4\pi$ ,  $v_{\max} = 10$ ,  $N_x = 128$ ,  $\Delta t = 5 \times 10^{-4}$ , and perturbation amplitude  $A = 0.5$ . This test has been studied in literature [4] as a fundamental test of the collisionless Landau damping and subsequent nonlinear evolution of the electrostatic field dominated by wave-particle interactions.

In this study, we apply the MM scheme only in the  $v$ -direction to check the velocity space resolution. In this case, the 0th-, 1st-, and 2nd-order moment variables correspond to the low-order discretized velocity moments, i.e., density, momentum and energy. They can reproduce the higher-order velocity moments balancing the transport flux in the quasi-steady state [8].

Figure 6 shows the deviation from the initial values of the entropy defined as  $S^n = -\sum_{i,j} f_{i,j}^n \ln f_{i,j}^n \Delta x \Delta v$  by the IDO-CF and MM schemes. It is important to consider the velocity space resolution of each scheme so that the mesh number in the  $v$ -direction can be changed as

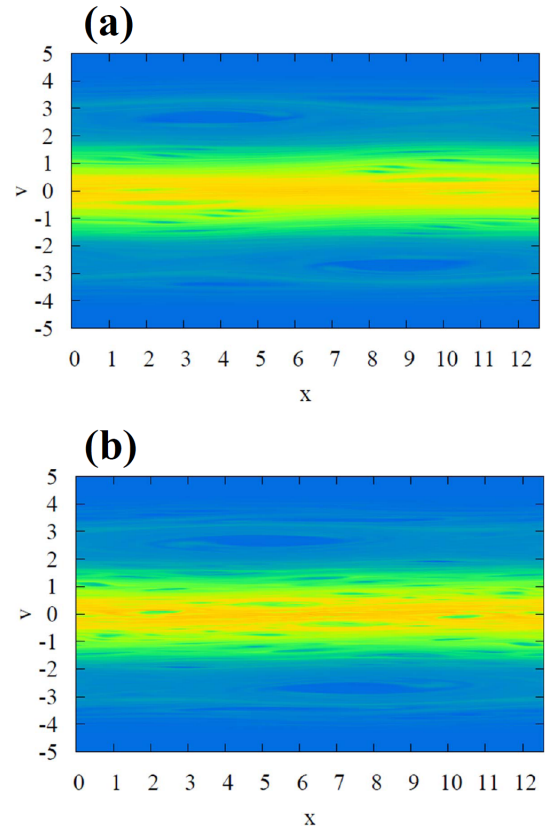


Fig. 7 Contour plots of the distribution function in phase space at  $t = 400$  by the (a) IDO-CF scheme with  $N_v = 2048$  and (b) MM scheme with  $N_v = 1024$ . Note that both cases have the same memory.

$N_v = \{1024, 2048\}$ . It is found that the typical time scale in which  $S$  begins to increase and also saturates is delayed by the MM scheme. Note that the IDO-CF scheme with  $N_v = 2048$  has the same memory as the MM scheme with  $N_v = 1024$ ; however, the increase of entropy becomes faster in the former case. This demonstrates that the MM scheme captures the finer scale structure in velocity space as is also observed in the contour plots of the distribution function shown in Fig. 7.

On the other hand, the MM scheme has the same total energy error level as the IDO-CF scheme. This originates from the fact that the error of the total energy is the most sensitive to  $\Delta x$ , which determines the resolution of the Poisson solver. Such a tendency is similar to that observed in Ref. [4].

## 7. Conclusion

In this paper, we have explored the MM scheme, which is an extension of the IDO-CF scheme, for solving the Vlasov-Poisson system. We have investigated the numerical properties of the MM scheme using the Fourier analyses and some benchmark tests of the 1D and 2D linear transport simulations. We found that both gain and phase of the MM scheme agree well with the ideal values up to the Nyquist wave number. We found that the MM scheme

can obtain less-dissipative and less-dispersive numerical results. The 1D Vlasov-Poisson simulations showed that the MM scheme captures the finer scale structure in velocity space, while also maintaining good energy conservation. These tests also showed that the MM scheme can be potentially extended to more realistic simulation such as gyrokinetic Vlasov simulation [1] which will be reported in a future publication.

## Acknowledgements

The authors would like to thank Prof. T. Utsumi of Tokyo University of Science, Yamaguchi for his valuable comments.

- [1] X. Garbet, Y. Idomura, L. Villard and T.-H. Watanabe, *Nucl. Fusion* **50**, 043002 (2010).
- [2] C.Z. Cheng and G. Knorr, *J. Comput. Phys.* **22**, 330 (1976).
- [3] Y. Imai, T. Aoki and K. Takizawa, *J. Comput. Phys.* **227**, 2263 (2008).
- [4] K. Imadera, Y. Kishimoto, D. Saito, J. Q. Li and T. Utsumi, *J. Comput. Phys.* **228**, 8919 (2009).
- [5] T. Utsumi, T. Kunugi and T. Aoki, *Comput. Phys. Commun.* **101**, 9 (1997).
- [6] Y. Imai and T. Aoki, *J. Comput. Phys.* **217**, 453 (2006).
- [7] S. T. Zalesak, *J. Comput. Phys.* **31**, 335 (1979).
- [8] T.-H. Watanabe and H. Sugama, *Phys. Plasmas* **9**, 3659 (2002).